

See discussions, stats, and author profiles for this publication at: <https://www.researchgate.net/publication/51035656>

Fluorescence Ratiometry and Fluorescence Lifetime Imaging: Using a Single Molecular Sensor for Dual Mode Imaging of Cellular Viscosity

ARTICLE *in* JOURNAL OF THE AMERICAN CHEMICAL SOCIETY · MAY 2011

Impact Factor: 12.11 · DOI: 10.1021/ja1104014 · Source: PubMed

CITATIONS

91

READS

91

11 AUTHORS, INCLUDING:



[Xiaojun Peng](#)

Dalian University of Technology

201 PUBLICATIONS 6,058 CITATIONS

[SEE PROFILE](#)



[Jingyun Wang](#)

Dalian University of Technology

74 PUBLICATIONS 2,117 CITATIONS

[SEE PROFILE](#)



[Jiangli Fan](#)

Dalian University of Technology

109 PUBLICATIONS 4,135 CITATIONS

[SEE PROFILE](#)



[Shiguo Sun](#)

Dalian University of Technology

123 PUBLICATIONS 3,629 CITATIONS


[SEE PROFILE](#)

Fluorescence Ratiometry and Fluorescence Lifetime Imaging: Using a Single Molecular Sensor for Dual Mode Imaging of Cellular Viscosity

Xiaojun Peng,^{*,†} Zhigang Yang,[†] Jingyun Wang,[†] Jiangli Fan,[†] Yanxia He,[†] Fengling Song,[†] Bingshuai Wang,[†] Shiguo Sun,[†] Junle Qu,[§] Jing Qi,[§] and Meng Yan[§]

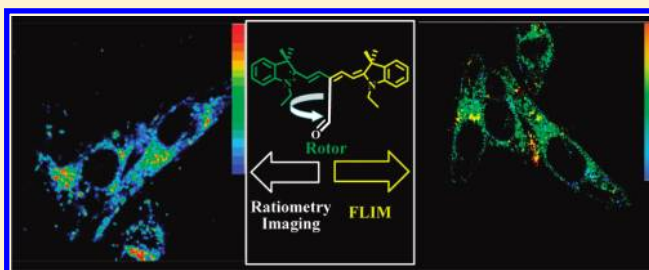
[†]State Key Laboratory of Fine Chemicals, [†]School of Life Science and Biotechnology, Dalian University of Technology, 2 Linggong Road, Hi-tech Zone, Dalian 116024, P.R. China

[§]Key Laboratory of Optoelectronic Devices and Systems of Ministry of Education, Shenzhen University, Shenzhen 518060, P.R. China.

 Supporting Information

ABSTRACT: Intracellular viscosity strongly influences transportation of mass and signal, interactions between the biomacromolecules, and diffusion of reactive metabolites in live cells. Fluorescent molecular rotors are recently developed reagents used to determine the viscosity in solutions or biological fluid. Due to the complexity of live cells, it is important to carry out the viscosity determinations in multimode for high reliability and accuracy. The first molecular rotor (RY3) capable of dual mode fluorescence imaging (ratiometry imaging and fluorescence lifetime imaging) of intracellular viscosity is reported.

RY3 is a pentamethine cyanine dye substituted at the central (*meso*-) position with an aldehyde group (CHO). In nonviscous media, rotation of the CHO group gives rise to internal conversion by a nonradiative process. The restraining of rotation in viscous or low-temperature media results in strong fluorescence (6-fold increase) and lengthens the fluorescence lifetime (from 200 to 1450 ps). The specially designed molecular sensor has two absorption maxima (λ_{abs} 400 and 613 nm in ethanol) and two emission maxima (in blue, λ_{em} 456 nm and red, 650 nm in ethanol). However it is only the red emission which is markedly sensitive to viscosity or temperature changes, providing a ratiometric response (12-fold) as well as a large *pseudo*-Stokes shift (250 nm). A mechanism is proposed, based on quantum chemical calculations and ¹H NMR spectra at low-temperature. Inside cells the viscosity changes, showing some regional differences, can be clearly observed by both ratiometry imaging and fluorescence lifetime imaging (FLIM). Although living cells are complex the correlation observed between the two imaging procedures offers the possibility of previously unavailable reliability and accuracy when determining intracellular viscosity.



■ INTRODUCTION

At the intracellular level, viscosity strongly influences intracellular transportation of mass and signal, interactions between biomacromolecules, and diffusion of reactive metabolites such as ROS and RNS. Changes in viscosity at cellular level relate to a number of diseases and pathologies.^{1,2} The existing mechanical methods—such as capillary viscometer, falling ball viscometer, and rotational viscometer for viscosity determination³—cannot provide measures of viscosity at a cellular level. In response to this, Luby-Phelps⁴ reported a ratiometric system of fluorescent Cy5 and Cy3 attached to macromolecular Ficoll 70 to measure intracellular viscosity. However, small molecule fluorescent sensors with cell-membrane permeability should be much more effective in the investigation of intracellular microviscosity.

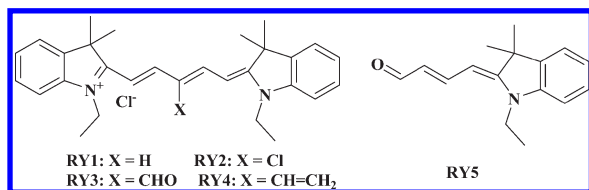
Recently developed molecular rotors are a group of fluorescent molecules that can be used to determine the viscosity in solutions or biological fluids. Such molecular rotors typically comprise a conjugated domain that can freely rotate in nonviscous or low-viscosity solutions, providing relaxation of the electronically excited dyes by nonradiative processes.^{5–10} Such

rotation can be restrained by viscous environments, following which the fluorescence intensity or lifetime of dyes will be seen to increase.

Fluorescence intensity-based measurements, however, are influenced by fluid optical properties, dye concentration, and other experimental or instrumental factors. A ratiometric approach, using probes that possess dual emission maxima from which the intensity ratio can be obtained, avoids most of the interferences^{11,12} and although influenced by viscosity the ratios are independent of the dye concentration.^{6,7,9} The fluorescence lifetimes of dyes are also independent of the interfering factors noted above. Moreover they do not even require calculation of the ratio, and offer easy system calibration together with ultra-sensitive detection.⁸ So fluorescence ratiometry and FLIM are ideal procedures for intracellular viscosity investigations. Theodorakis^{6,7} and Suhling^{8–10,13} have reported on some fluorescent molecular rotors and have made good progress regarding

Received: November 28, 2010

Published: April 08, 2011

Scheme 1. Structures of **RY3** and Related Compounds

the investigation of intracellular viscosity. In practical applications, however it is important that intracellular viscosity detection can use both fluorescence ratiometry and lifetime detection, to provide high reliability and accuracy. Up to now, however, there is no such dual-mode molecular sensor could be used to detect viscosity and map intracellular viscosity by both ratiometric imaging and FLIM.

Here we report a fluorescent molecular rotor, **RY3** (Scheme 1, X = CHO). This provides two emission peaks: one in the blue region (λ_{em} 456 nm, in EtOH), and one in the red (λ_{em} 650 nm, in EtOH). Fluorescence is very weak in nonviscous environments. However on increasing viscosity, the red emission is greatly enhanced while the blue emission remains insensitive, providing the basis for a ratiometric procedure. In parallel to this, the fluorescence lifetime for the red emission is also markedly prolonged in viscous media, from 200 ps to more than 1400 ps. **RY3** is the first fluorescent molecule which can be used as dual-mode molecular fluorescence sensor in both fluorescence ratiometry and lifetime fluorescence detection.

EXPERIMENTAL SECTION

Sample Preparation. 2, 3, 3-trimethyl-3H-indole, indolenium quaternized salts¹⁴ and other intermediates^{15,16} were prepared according to literature methods. The preparation procedures of **RY1-RY5** and related intermediates are given in the Supporting Information (SI). All solvents and reagents used were reagent grade. All reactions were carried out under a nitrogen atmosphere with dry, freshly distilled solvents under anhydrous conditions. Silica gel (100–200 mesh) was used for flash column chromatography for purifications. Bovine Serum Albumin (BSA) was purchased from Shanghai Sangon Biotech Co., Ltd. Water used in all experiments was doubly purified by Milli-Q Systems equipment. The solutions of **RY1-RY5** were typically prepared from 1.0 mM stock solutions in DMSO.

Quantum Calculations. All the quantum-chemical calculations were done with the Gaussian 09 suite.¹⁷ The parameter referred to the work of Han.¹⁸ The geometry optimizations of the dyes were performed using density functional theory (DFT)¹⁹ with Becke's three-parameter hybrid exchange function with Lee–Yang–Parr gradient-corrected correlation functional (B3-LYP functional) and 6-31G ** basis set. No constraints to bonds/angles/dihedral angles were applied in the calculations and all atoms were free to optimize. The electronic transition energies and corresponding oscillator strengths were calculated with time-dependent density functional theory (TD-DFT)^{20,21} at the B3LYP/6-31G ** level.

Absorption and Fluorescence Quantum Yields Measurements. Absorption spectra were measured on a Lambda LS35 spectrophotometer. Fluorescence spectra were obtained with a FP-6500 spectrophotometer (Jasco, Japan). The relative fluorescence quantum yields were determined with Rhodamine B as a standard²² and calculated using the following equation:

$$\Phi_x = \Phi_s(F_x/F_s)(A_s/A_x)(\lambda_{\text{exs}}/\lambda_{\text{exx}})(n_x/n_s)^2$$

where Φ represents quantum yield; F stands for integrated area under the corrected emission spectrum; A is absorbance at the excitation wavelength; λ_{ex} is the excitation wavelength; n is the refractive index of the solution (because of the low concentrations of the solutions (10^{-7} – 10^{-8} mol/L), the refractive indices of the solutions were replaced with those of the solvents); and the subscripts x and s refer to the unknown and the standard, respectively.

Viscosity Determination, Fluorescence Spectral Measurement, and Fluorescence Lifetime Detection. The solvents were obtained by mixing ethanol-glycerol, methanol-glycerol, and deionized water-glycerol systems in different proportions. Measurements were carried out with a NDJ-7 rotational viscometer, and each viscosity value was recorded. The solutions of **RY1-RY5** of different viscosity were prepared by adding the stock solution (1.0 mM) to 10 mL of solvent mixture (ethanol-glycerol, water-glycerol, and methanol-glycerol solvent systems) to obtain the final concentration of the dye (1.0 μM). These solutions were sonicated for 5 min to eliminate air bubbles. After standing for 1 h at a constant temperature, the solutions were measured in a UV spectrophotometer and a fluorescence spectrophotometer. A fluorescence lifetime measuring equipment (Horiba Jobin Yvon Fluoromax-4p) was used to obtain the fluorescence lifetimes of **RY3**, with the excitation wavelength at 376 nm and detection at 650 nm.

Low Temperature ¹H NMR and Fluorescence Spectra. The temperatures of solutions were slowly lowered from 25 °C by liquid nitrogen to 0 °C, –25 °C, and –50 °C. The ¹H NMR spectra of **RY1** and **RY3** in CDCl₃ were obtained using a nuclear magnetic resonance spectrometer (Varian INOVA 400 MHz). Fluorescence spectra of **RY1-RY4** were measured on a FP-6500 spectrophotometer (Jasco, Japan), with the excitation wavelength fixed at 600 nm. **RY3** (1.0 μM) in 70% glycerol–water mixture was measured on the fluorescence spectrophotometer at –5 °C, 0 °C, 5 °C...40 °C with excitation wavelength of 400 nm, and the fluorescence lifetimes of **RY3** at the same temperature were measured.

Cell Incubation and Imaging. PC12, MCF-7, and NIH-3T3 cells were cultured in DEME (Invitrogen) supplemented with 10% FCS (Invitrogen). One day before imaging, cells were seeded into 24-well flat-bottomed plates. The next day, the cells were incubated with 5.0 μM dye for 0.5 h at 37 °C under 5% CO₂ and washed with phosphate-buffered saline (PBS) three times. Fluorescence imaging of PC12 cells was carried out using a Nikon Eclipse TE2000–5 inverted fluorescence microscope with a 10 \times objective lens (excited with green light). MCF-7 cells were incubated with **RY3** and observed under a Leica TCS-SP2 confocal fluorescence microscope, 100 \times objective lens. Then the fluorescence intensity and fluorescence lifetime of **RY3** in NIH-3T3 cells were observed under a Leica TCS-SP2 confocal fluorescence microscope and TCSPC FLIM equipment (SPC150) at 4 °C, 20 °C, and 37 °C.

Titration by Bovine Serum Albumin (BSA) and Cysteine. The stock solution of **RY3** (1.0 mM) was diluted by 20.0 mM phosphate buffer solution (PBS, pH 7.4) to obtain a solution with concentration of 2.0 μM . BSA was dissolved in doubly purified water with a concentration of 50.0 mg/mL. The BSA solution was gradually added to the **RY3** solution, over the range 0–2.0 mg/mL. The solution obtained was left to stand to eliminate air bubbles, and measured in the UV spectrophotometer and fluorescence spectrophotometer. When finishing the titration with a BSA concentration of 2.0 mg/mL, the solution was stood at 37 °C for 120 min, then the absorption and fluorescence spectra were measured on the spectrometer every 10 min to examine the spectra changes of **RY3** upon addition of BSA.

The similar titrations of **RY3** (2.0 μM) by cysteine (25.0 mM) was carried out under the same conditions as that using BSA, the final concentration of cysteine being 200 μM . After the titration, the solution was stood at 37 °C for 120 min, then the absorption and fluorescence spectra were measured on the spectrometer every 10 min to check for any spectral changes of **RY3** upon addition of cysteine.

Photostability. **RY1-RY4** were dissolved in DMSO–water (5:5 v/v) at a concentration of 10.0 μM , respectively. The solutions were irradiated

Table 1. Spectral Data of the Dye RY1–RY4 in Different Solvents

dyes	solvents	dielectric constant	η^a (cP)	$\lambda_{\text{abs}}^{b,c}$ (nm)	$\lambda_{\text{em}}^{b,d}$ (nm)	$\epsilon^{b,e}$	$\Phi_f^{b,f}$
RY1	THF	7.43	0.53	653	662	2.27	0.37
	DCM	8.93	0.43	661	671	3.06	0.29
	ethanol	24.85	1.20	652	663	3.02	0.27
	methanol	32.61	0.59	649	659	2.59	0.22
	DMSO	46.83	2.00	655	668	2.72	0.33
	H ₂ O	78.36	1.01	648	656	2.27	0.13
RY2	THF	7.43	0.53	657	661	1.86	0.12
	DCM	8.93	0.43	663	669	2.00	0.11
	ethanol	24.85	1.20	654	659	2.00	0.10
	methanol	32.61	0.59	649	656	1.97	0.09
	DMSO	46.83	2.00	656	663	1.76	0.25
	H ₂ O	78.36	1.01	648	654	1.36	0.05
RY3	THF	7.43	0.53	(399) 617	(455) 651	(0.16) 1.02	(0.006) 0.03
	DCM	8.93	0.43	(399) 624	(454) 649	(0.11) 1.05	(0.006) 0.04
	ethanol	24.85	1.20	(400) 613	(456) 650	(0.15) 1.10	(0.005) 0.03
	methanol	32.61	0.59	(400) 609	(450) 648	(0.13) 1.11	(0.004) 0.02
	DMSO	46.83	2.00	(400) 613	(451) 630	(0.14) 1.10	(0.010) 0.07
	H ₂ O	78.36	1.01	(413) 600	(460) 638	(0.15) 0.77	(0.002) 0.02
	A1 ^g			(400)606	(453)654	(–)1.04	(–) 0.067
	A2 ^g			(399)604	(454)652	(–)1.02	(–) 0.059
	A3 ^g	45.8	950	(398)608	(461)650	(–)0.83	(–) 0.181
RY4	THF	7.43	0.53	690	706	1.2	0.09
	DCM	8.93	0.43	695	708	2.4	0.11
	ethanol	24.85	1.20	684	704	2.1	0.07
	methanol	32.61	0.59	681	702	2.2	0.05
	DMSO	46.83	2.00	688	710	2.1	0.17
	H ₂ O	78.36	1.01	680	697	1.5	0.04

^a The viscosity data of the solvents were measured at 25 °C. ^b There are two group of absorption and emission peaks for RY3; and the data in the parentheses are the absorption, emission wavelengths, molar extinction coefficient, and fluorescence quantum yields of RY3 at the second peak. ^c The absorption peaks of dyes (nm). ^d RY3 was excited at 400 nm, and other dyes were excited at their maximum absorption wavelengths. ^e $\times 10^5 \text{ mol}^{-1} \text{ cm}^{-1} \text{ L}$. ^f Rhodamine B was used as a standard reference with a fluorescence quantum yield of 0.97 in ethanol, errors were estimated to be 10% for fluorescence quantum yield. ^g The fluorescence quantum yields of RY3 at 650 nm in the mixture solvents and 99% glycerol were just considered; A1, ethanol-glycerol (1: 1 v/v); A2, methanol-glycerol (1: 1 v/v); A3, 99% glycerol.

under a 500 W iodine–tungsten lamp for 7 h at a distance of 250 mm away. An aqueous solution of sodium nitrite (50.0 g/L) was placed between the samples and the lamp as a light filter (to cut off the light shorter than 400 nm) and heat filter. The photostabilities were expressed in the terms of remaining absorption (%) calculated from the changes of absorbance at the absorption maximum before and after irradiation by iodine–tungsten lamp.

Redox Potential Measurements. The redox potential (cyclic voltammetry, CV; and differential pulse voltammetry, DPV) was measured using a BAS 100B electrochemical analyzer. A three-electrode cell was composed of a glass-carbon as working electrode, a platinum wire as counter electrode, and Ag/AgCl as reference electrode (10.0 mM AgNO₃). The supporting electrolyte was TBAPF₆ (0.1 M tetra *n*-butylammonium hexafluorophosphate) and the concentrations of RY1–RY4 were 1.0 mM in acetonitrile.

RESULTS AND DISCUSSION

Spectral Properties. The four pentamethine dyes (RY1–RY4) have different substituents (H, Cl, CHO, and CH=CH₂ respectively) at the central (*meso*-) position of the pentamethine

chain.^{23,24} As seen in Table 1, three dyes (RY1, RY2, and RY4) possess only one group of absorption (λ_{abs}) and fluorescence (λ_{em}) peaks: RY1 (λ_{abs} 652 nm and λ_{em} 663 nm in ethanol), RY2 (λ_{abs} 654 and 659 nm in ethanol), and RY4 (λ_{abs} 684 nm and λ_{em} 704 nm in ethanol), respectively. However, RY3, with an aldehyde substituent at the *meso*-position of the pentamethine chain, has two absorption peaks (λ_{abs} 400 and 613 nm in ethanol) and two emission peaks (λ_{em} 456 and 650 nm in ethanol). Compared with RY1 and RY5 (Figure 1), the spectrum of RY3 has a short wavelength peak similar to RY5 (λ_{abs} 415 and λ_{em} 466 nm), and a wavelength peak similar to RY1. For the red emission RY4, with a conjugated electron-donating vinyl group, has the longest wavelength; whereas RY3, conjugated with an electron-withdrawing CHO group, has the shortest wavelength. The molar extinction coefficient (ϵ) of RY3 is also the smallest (about $1.0 \times 10^5 \text{ mol}^{-1} \text{ cm}^{-1} \text{ L}$), only half that of other dyes. So dye RY3 must have a unique emission mechanism. Note that a low quantum yield corresponds to a low nonsignal background, when fluorescence enhancement in the target will provide a good signal-to-noise ratio.

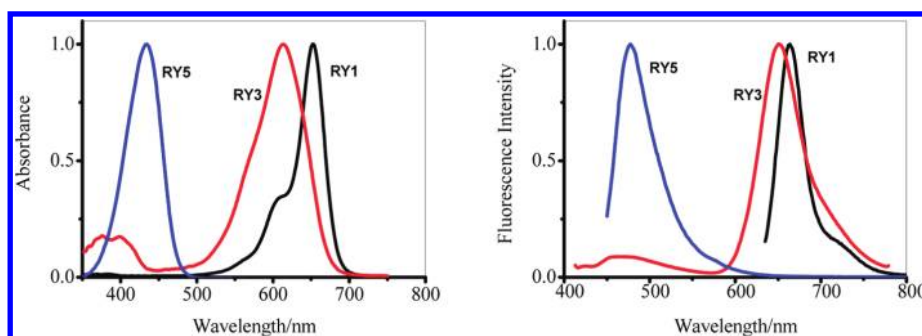


Figure 1. The normalized absorption (Left) and emission (Right) spectra of dyes RY1, RY3, and RY5 in 99% glycerol.

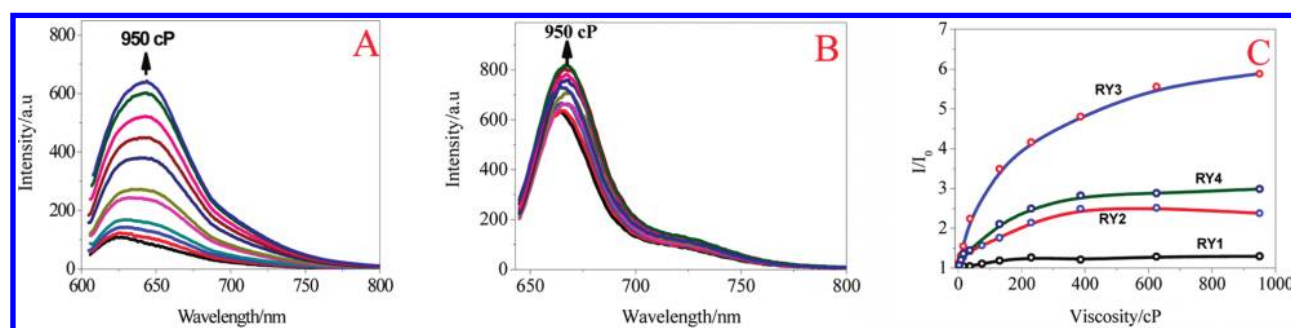


Figure 2. The fluorescence spectra of RY3 (A), RY1 (B), and the comparison of fluorescence increase fold of different dyes with the increase of solution viscosity (C), RY3 was excited at 600 nm and RY1, RY2, and RY4 were excited at the maximum absorption peaks.

Generally solvents with different polarity always influence the wavelengths and quantum yields to some extent. However for RY3, the influence was very limited. In a set of dielectric constant values ranging from 7.43 (THF) to 78.36 (H₂O), the quantum yields of RY3 showed little change (0.03 in THF and 0.02 in H₂O). This means that, in nonviscous solvents, the polarity of the solvents has little effect on fluorescence quantum yields. This characteristic is crucial for a molecular rotor to sense environmental viscosity, while excluding the influence of polarity.²⁵

Fluorescence Response to Solvent Viscosity. Unlike its insensitivity to polarity, the fluorescence of RY3 was more sensitive to solution viscosity than the other three dyes. By adding glycerol to the ethanol solution of RY3, the viscosity of the solution was increased from 1.2 cP (ethanol) to 950 cP (99% glycerol). As the viscosity increased, fluorescence of RY3 was greatly enhanced by 6 fold in quantum yield (0.03 in ethanol and 0.181 in 99% glycerol in Table 1), although its absorbance showed almost no change. With increasing proportions of glycerol in the mixture solvent, the fluorescence intensity of RY3 at 650 nm increased continuously (Figure 2A), until close to the intensity of RY1 (Figure 2B). Other dyes did not show such fluorescence enhancement under the same conditions: RY1 (0.25 fold), RY2 (1.5 fold), and RY4 (1.9 fold) (Figure 2C).

The quantitative relationship between the fluorescence intensity I_f of a molecular rotor and the viscosity η of the solvent is well expressed by the Förster–Hoffmann eq 1:²⁶

$$\log I_f = C + \alpha \log \eta \quad (1)$$

where C is a concentration- and temperature-dependent constant and α is a dye- and temperature-dependent constant. RY3 fits the linear relationship between $\log I_f$ and $\log \eta$ ($R^2 = 0.991$,

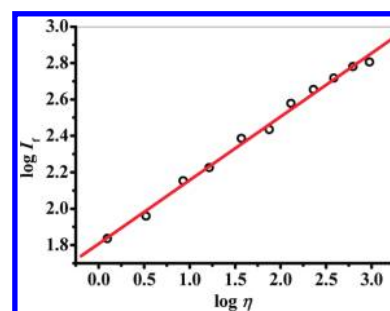
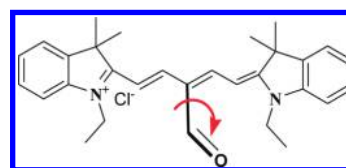


Figure 3. The linearity of $\log I_f$ versus $\log \eta$ plot of RY3 (1.0 μ M) in ethanol-glycerol mixed solvents, excited at 600 nm.

Scheme 2. Hypothetical Rotation of CHO Group



$\alpha = 0.30$, λ_{em} 650 nm) (Figure 3). RY1, with hydrogen atom at the *meso*-position, has little response ($\alpha = 0.04$).

The difference in sensitivity may be attributed to the different substituents (X) at the central position of the polymethine-chain of the dyes. In the case of RY1 ($X = H$) the dye has high quantum yield in most solvents with different viscosity, so this kind of dye is good for fluorescent labels but not for good viscosity sensing. Where bulky substituents (RY3 ($X = CHO$) and RY4

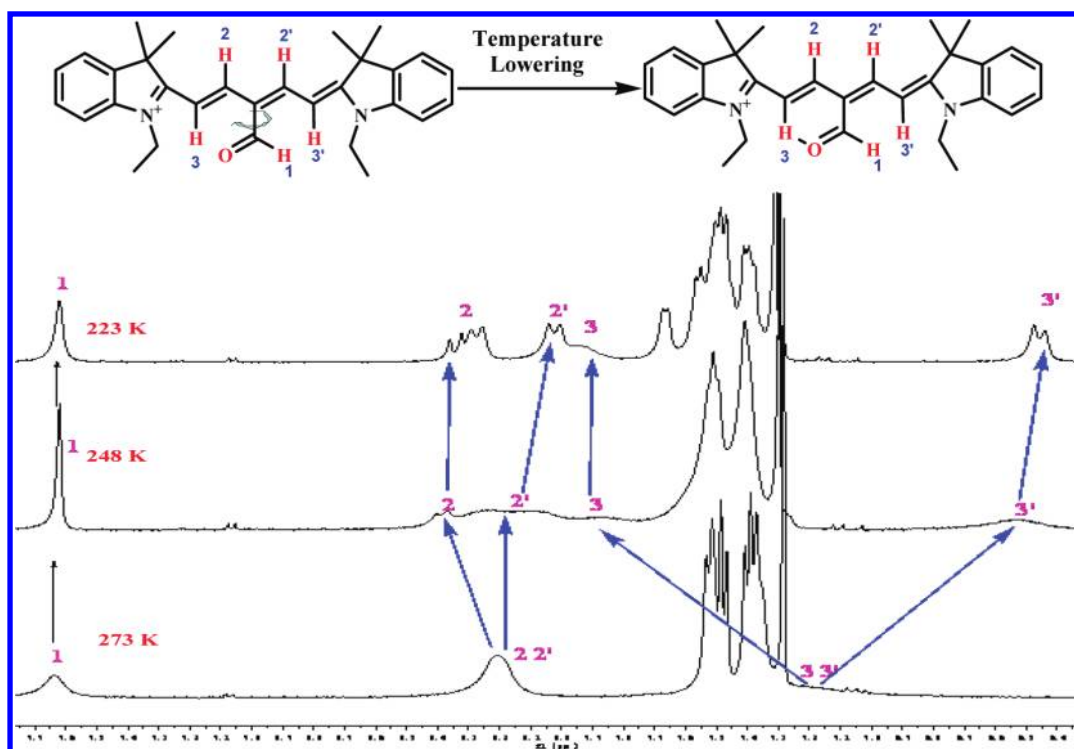


Figure 4. NMR evidence for restricted rotation of the aldehyde group at low temperature, and the interaction between the oxygen and adjacent hydrogen atom at pentamethine chain (above), note the split of the H-chemical shift of conjugated chain of **RY3** in CDCl_3 at different temperature (0°C , -25°C , and -50°C) (below).

($\text{X} = \text{CH}=\text{CH}_2$) are present, then these groups may rotate^{5–9} (Scheme 2) or vibrate to change the geometry of the molecule in the excited state. In nonviscous solution, these changes occur readily, and permit the excited state to relax by a nonradiative process, reducing the quantum yield. In viscous solution, however, this change is restrained, so the fluorescence quantum yield or intensity should increase. It is possible that the CHO group in **RY3** rotates around the C—C bond more easily than does the vinyl group in **RY4**. Alternatively the electron-withdrawing character of CHO results in ICT (internal charge transfer), so **RY3** has a lower fluorescence background and better enhancement than **RY4**.

Fluorescence Increase at Low Temperature. Similar to the restricted rotation of the CHO of **RY3** in high-viscous solutions, lowering the temperature of nonviscous solutions could also retard the rotation of the CHO group. Chloroform was chosen as the solvent to avoid interference from hydrogen bonding between solvent molecules and the CHO group. As shown in SI Figure S1A, from 25°C to -50°C , enhancement of fluorescence intensity of **RY3** in chloroform increased nearly 4 fold. Little enhancements for **RY1**, **RY2**, and **RY4** were found under the same conditions (SI Figure S1B).

The rotation of CHO group can be inferred from the ^1H NMR at low temperature. At -50°C , the rotation of the CHO group of **RY3** slows down. This results in a different interaction with its adjacent hydrogen atom at the pentamethine chain, such as possible hydrogen bond interaction between the oxygen atom of aldehyde group with H_3 shown in Figure 4, where H_3 and H_3' shift to 7.95 and 6.45 from 7.28 ppm (at -50°C); H_2 and H_2' also shift to 8.31 and 8.03 from 8.20 ppm (at -50°C). As the shifts of H_3/H_3' are much larger than H_2/H_2' , the action of the oxygen atom of the CHO group on spatially fitted H_3/H_3' is more

intense than H_2/H_2' . At higher temperature (0°C), the free rotation of the CHO group generates no such split. **RY1**, even at low temperature (-25°C and -50°C), has no split or shift in ^1H NMR (SI Figure S2) and little fluorescence change.

Ratiometric Fluorescence of **RY3.** As illustrated in Figure 1, **RY3** possesses a unique spectral character, with two emission peaks (such as λ_{em} 456 and 650 nm in ethanol). Most importantly only the red emission of **RY3** responded significantly to the viscosity of the solvent. As shown in Figure 5 and SI Figure S3, in different viscous solvent systems (ethanol-glycerol (Figure 5A), water-glycerol (Figure 5C) and methanol-glycerol (SI Figure S3)), the red fluorescence intensity at 650 nm increased sensitively with viscosity of the solvents. The blue emission at 456 nm, however, gave only very small responses. This permits ratiometric changes with a linear relationship between $\log(I_{650}/I_{456})$ and $\log \eta$. This is fitted by the Förster–Hoffmann equation, R^2 of the linear relation increases in the ethanol-glycerol system (Figure 5B) and water-glycerol system (Figure 5D) were 0.989 and 0.99, and the slope α are 0.30 and 0.38, respectively. This demonstrated that **RY3** could be employed to ratiometrically detect the solution viscosity.

When the temperature was reduced from 40°C to -5°C , the fluorescence intensity at 650 nm was enhanced many fold, while the blue emission at 456 nm showed little increase (Figure 6A). Similarly the ratio linearity between $\log(I_{650}/I_{456})$ and temperature was obtained (Figure 6B). This shows that cooling has the similar effect as viscosity in restraining the rotation of the CHO group.

Theoretical Calculation and Mechanism. The structural optimization of **RY3** by DFT/TDDFT in B3LYP/6-31G** level of Gaussian 09 (the atomic standard orientations after geometry optimization of ground state and excited state have been given in

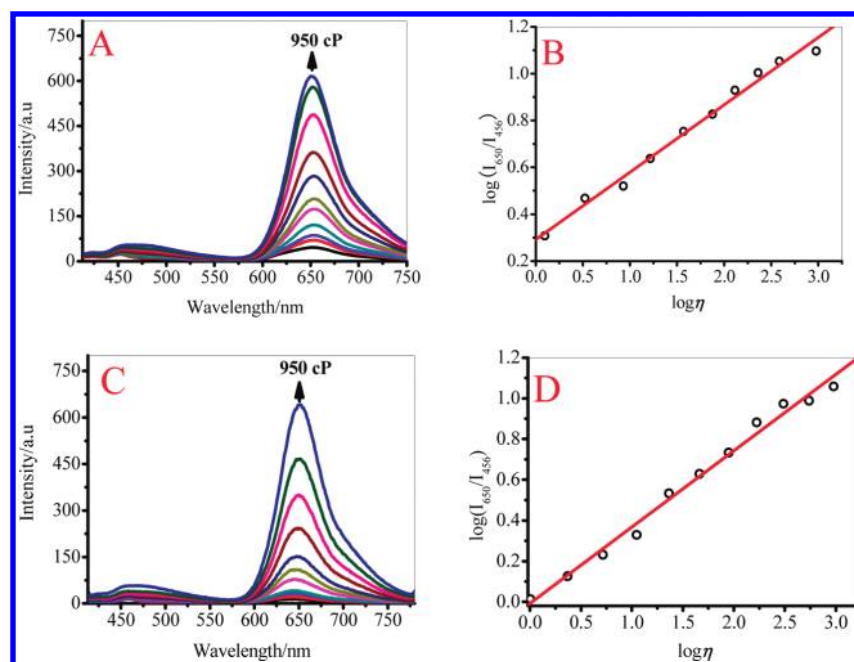


Figure 5. The emission spectra changes of RY3 (1.0 μM) with the increase of the viscosity of solvent and the linear response between $\log(I_{650}/I_{456})$ and $\log \eta$ in the solvent of ethanol-glycerol (A and B) and water-glycerol (C and D), excited at 400 nm.

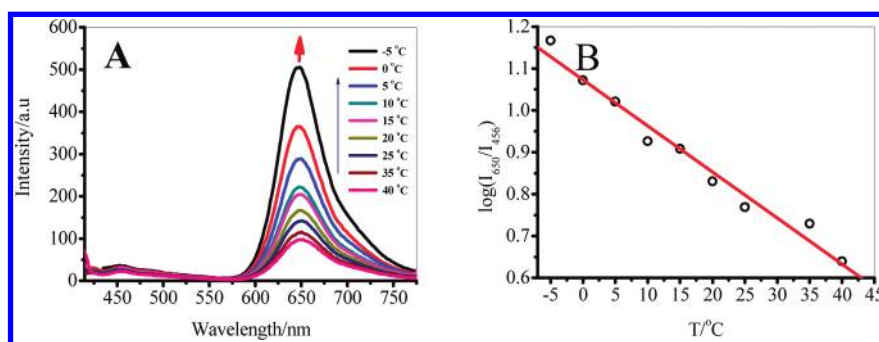


Figure 6. The fluorescence spectra and ratio of RY3 (1.0 μM) at different temperatures in water-glycerol (30/70, v/v), excited at 400 nm (A); and the linearity of the plot of $\log(I_{650}/I_{456})$ versus temperature (B).

Supporting Information), is shown in Figure 7. Two main electronic transitions ($S_0 \rightarrow S_1$, oscillator strength $f_{ab} = 1.75$; and $S_0 \rightarrow S_2$, oscillator strength $f_{ab} = 0.15$) were obtained, corresponding to the two absorption peaks (λ_{abs} 613 and 400 nm in ethanol). The two main electronic transitions from excited state ($S_1 \rightarrow S_0$, oscillator strength $f_{em} = 2.08$; and $S_2 \rightarrow S_0$, oscillator strength $f_{em} = 0.17$), corresponded to two emission (λ_{em} 650 and 456 nm in ethanol) peaks of RY3. The short absorption and emission (λ_{abs} 400 nm and λ_{em} 456 nm) have very small oscillator strength (f_{ab} 0.15 and f_{em} 0.17 respectively), corresponding to the low molar extinction coefficient (ϵ) and fluorescence quantum yields (Figure 1 and Table 1).

When RY3 was excited at 400 nm, the dye molecules underwent a transition to the second excited state (S_2), accompanied by intramolecular charge transfers (ICT). There are two competing decay processes from the excited state S_2 . The first is fluorescence emission where the electron returns to ground state (S_0) directly from S_2 with a blue fluorescence emission (λ_{em} 456 nm). The second is internal conversion where the molecule is relaxed to the first excited state (S_1). This second decay mechanism, internal

conversion, is a rapid process (femto- or pico-second) compared to fluorescence emission (nanosecond). Consequently the most likely outcome is to transfer to the first excited state by internal conversion ($S_2 \rightarrow S_1$). According to the classic “energy gap law” (the smaller the energy gap, the greater the possibility of internal conversion), internal conversion $S_2 \rightarrow S_1$ is much easier than that of $S_2 \rightarrow S_0$.

Similarly with S_2 , the S_1 state also decays to S_0 via two competing mechanisms, fluorescence emission and internal conversion. In nonviscous solution (Figure 8A), the rotation of the CHO group raises the vibrational energy, consequently internal conversion is the favored mechanism, and it dominates the decay. However in viscous or cooled media (Figure 8B), the rotation is restricted, so fluorescence emission dominates. This emission ($S_1 \rightarrow S_0$) contributes to the strong red fluorescence of λ_{em} 650 nm occurring in viscous media or at low temperature.

Therefore, a ratio increase (I_{650}/I_{456}) with viscosity or temperature results from the different internal conversions controlled by the energy gap law and influenced by CHO rotation. The energy gap law allows internal conversion to predominate

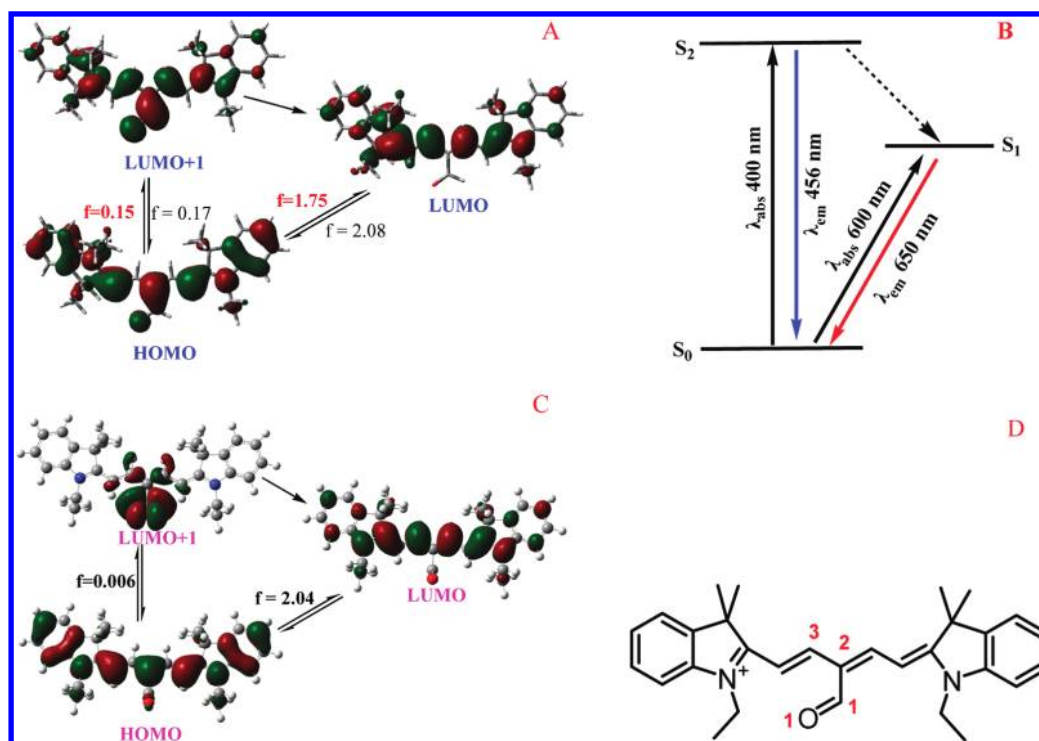


Figure 7. Frontier molecular orbital (MO) of **RY3** calculated with time-dependent density functional theory (TDDFT) at the B3LYP/6-31G** level (number of states: 6) using Gaussian 09: A, the dihedral angle of O1C1C2C3 is ca. 0°; B, the proposed diagram of the energy levels of **RY3**; C, the dihedral angle of O1C1C2C3 is ca. 90°; and D, the dihedral angle of O1C1C2C3 is figured in the structure of **RY3**.

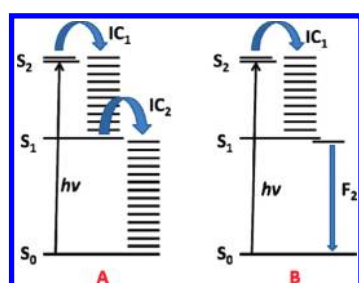


Figure 8. The schematic illustration of the decay processes of **RY3** in nonviscous (A) and viscous or cooled media (B). IC₁ and IC₂ are two internal conversion processes. F₂ is the emission of λ_{em} 650 nm.

when there is a small energy gap between two energy levels. The CHO-rotation enhances the internal conversion by raising the vibration energy. The blue emission (λ_{em} 456 nm) of **RY3** is from the electron transition $S_2 \rightarrow S_0$ which is only slightly influenced by CHO rotation as the energy gap ($S_2 - S_0$) is relatively large. By contrast, the red emission (λ_{em} 650 nm) of **RY3** is from the electron transition $S_1 \rightarrow S_0$ which is strongly influenced by CHO rotation as the energy gap ($S_1 - S_0$) is rather small and sensitive to the vibrational change. The fast internal conversion of $S_2 \rightarrow S_1$ provides the major transient species of S_1 and increases the probability of red emission. These processes are illustrated in Figure 8.

With similar calculation, by DFT/TDDFT in B3LYP/6-31G** level of Gaussian 09, compared with **RY3**, **RY4** shows different results. The oscillator strength for the electron transition from HOMO (S_0) to LUMO+1 (S_2) is only 0.0075, compared to the normal electron jump from HOMO (S_0) to LUMO (S_1) with an oscillator strength of 1.90. So, short wavelengths (absorption and

emission) are prohibited and only one set of absorption and emission peaks with long wavelength has been observed in the spectra of **RY4**.

The above results arise from the key action of CHO group in **RY3**. Because of the electron-withdrawing effect, CHO induces an internal charge transfer process (ICT). The LUMO+1 of **RY3** (S_2 , Figure 7A) clearly shows the unequal distribution of charge. In particular when CHO group rotates, for example twists to 90° where the electron cloud density increases markedly on the CHO group at the LUMO+1 level (Figure 7C), twisted intramolecular charge transfer (TICT) might occur. This would enlarge the fluctuation in vibration energy level and increase the possibility of internal conversion which is sensitive to the viscosity and the temperature of media.⁵ The low molar extinction coefficients of **RY3** (Table 1) is the further evidence for the ICT processes.

The effect of CHO group also can be seen in the case of **RY5**. The fluorescence of **RY5** shows a 10-fold enhancement from ethanol to 99% glycerol (SI Figure S4), whereas **RY1** has no such response under the same conditions.

Fluorescence Lifetime. As reported by Suhling et al.,^{10–13} FLIM is another good way to investigate the intracellular viscosity and is also independent of the concentration of the dye. The quantitative relationship between the fluorescence lifetime (τ_f) of molecular rotor and viscosity (η) of the solvent is well depicted by Förster–Hoffmann eq 2:²⁶

$$\log \tau_f = C + x \log \eta \quad (2)$$

where C is a concentration- and temperature-dependent constant and x is a dye- and temperature-dependent constant.

As shown in Figure 9A, when the proportion of glycerol in the solvent mixture increases, and especially when the glycerol

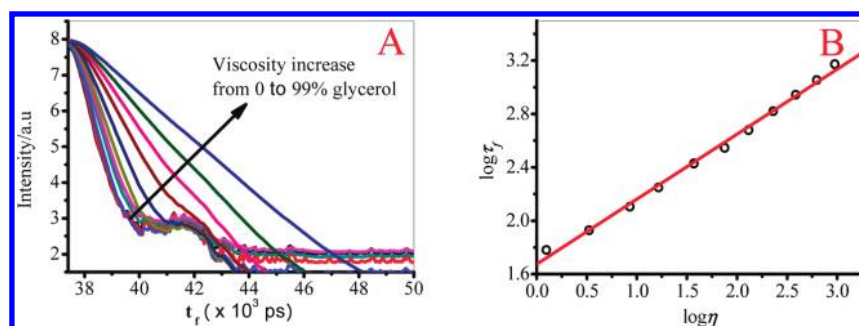


Figure 9. The fluorescence lifetime of RY3 (1.0 μ M) changes with viscosity of solvents at 650 nm. (A) Fluorescence decays as a function of viscosity by increasing the proportions of glycerol in ethanol-glycerol solutions (with a Horiba Jobin Yvon Fluoromax-4p system excited at 376 nm); and (B) the linearity between $\log \tau_f$ and $\log \eta$.

proportion is over 70%, the lifetime (τ_f) gradually becomes longer. From pure ethanol to 99% glycerol, the total fluorescence lifetimes of RY3 increased from 200 to 1450 ps, with a linear relationship between $\log \tau_f$ and $\log \eta$ (Figure 9B) ($R^2 = 0.996$) and large slope ($\alpha = 0.49$), giving a good fit with the Förster–Hoffmann eq 2.

In a 70/30 glycerol–ethanol solution, as the temperature is increased from 5 to 40 $^{\circ}$ C, the fluorescence decay becomes faster (Figure 10). The fluorescence lifetime of RY3 was shortened from 711.2 to 183.6 ps in a clearly linear inverse relationship between $\log \tau_f$ and temperature with R^2 0.996. This is expected because the viscosity of a solution is inversely proportional to temperature.

Possible Influences from Proteins and Photodecomposition. Proteins and mercapto-containing amino acids such as cysteine sometimes react with aldehydes.^{27–29} Regarding the importance of CHO in RY3, it is important to establish whether RY3 reacts with such biochemicals intracellularly. When RY3 (2.0 μ M) in PBS solution (pH 7.4) is titrated with 0–2.0 mg/mL BSA (SI Figure S5) or cysteine (0–200 μ M, SI Figure S6), the changes in absorbance (except for a new absorption peak of BSA at 280 nm), fluorescence intensity, and fluorescence ratio are all negligible, even after the mixture is stirred at 37 $^{\circ}$ C for more than 120 min. Comparing the results with and without BSA, under similar reaction conditions, the ratio values (I_{650}/I_{456}) (SI Figure S7) and the fluorescence lifetimes (SI Figure S8) of RY3 have similar linear relationships.

It is not surprising, as most of the aldehydes reactive with proteins or mercapto-containing acids are aliphatic aldehydes. However, RY3 is an aromatic aldehyde, and such species are rather stable in neutral aqueous media.

Additionally, poor photostability is a general drawback of polymethine dyes. It has been suggested that singlet oxygen ($^1\text{O}_2$) and super oxide anion ($\text{O}_2^{\cdot-}$) oxidize excited dye molecules under light irradiation.^{30–33} As SI Figure S9 shows, however, RY3 displayed excellent photostability. After irradiation by a 500 W iodine–tungsten lamp for 7 h, the absorption of RY3 remained as high as 95.9%, while other dyes were less stable: RY1 (50.4%), RY2 (85.1%), and RY4 (4.1%), respectively. This might result from the electron-withdrawing effect of the CHO group which decreases the electron density in the pentamethine chain of RY3. The order of first oxidization potential values (SI Table S1) of these dyes—0.71 V (RY3) > 0.55 V (RY2) > 0.41 V (RY1) > 0.20 V (RY4)—supports the above viewpoint. So RY3, with excellent photostability, is an ideal candidate for laser confocal imaging.

Dual Mode Fluorescence Imaging. Cyanine dyes have been widely used as fluorescence sensors^{34–36} and some have been used for imaging in vivo.^{37–39} However, the ratiometric system is rather rare.^{40,41} RY3 can penetrate live cell membranes, and image viscosity in cytoplasmic structures of living cells; such as PC12 cells shown in SI Figure S10, breast cancer cells MCF-7 in SI Figures S11, S12 and NIH-3T3 cells in SI Figure S13. After MCF-7 cells were incubated with RY3 (5.0 μ M), clear fluorescence images at 650 ± 20 nm map the cellular viscosity (SI Figure S12B). In the blue channel ($\lambda_{\text{em}} 456 \pm 20$), however, the fluorescence image is very weak (SI Figure S12A). The ratio image ($I_{650 \pm 20}/I_{456 \pm 20}$) displays the different viscosity areas in MCF-7 cells and is independent of the concentration or distribution of the dyes (Figure 11). In most imaging areas of MCF-7 cells are blue, with small ratio values, and low viscosity (less than 100 cP); some regions are green, indicating an intermediate ratio value of 100–400 cP of viscosity; and the small intracellular red zone indicates larger ratio values and higher viscosity, of more than 900 cP, which can be estimated by the calibration linearity between $\log(I_{650 \pm 20}/I_{456 \pm 20})$ and $\log \eta$.

Using a time-correlated single photon counting (TCSPC) system,^{42,43} and RY3, a fluorescence lifetime image (Figure 12) for cellular viscosity was obtained. It can be seen that some of cellular regions are colored cyan, indicating that the fluorescence lifetime of RY3 in those areas is less than 500 ps (or 100 cP). The main part (green region) represents the fluorescence lifetime of RY3 inside cells around 500–800 ps, corresponding to the viscosity value of 100–400 cP. In some small orange areas of the cells, the lifetime is as long as ca. 1800 ps (ca. 900 cP), close to 99% glycerol solution (1450 ps, or 950 cP).

To check the reliability, we changed the testing temperature from 4 to 37 $^{\circ}$ C. RY3 shows similar changes in ratio values and fluorescence lifetimes. As shown in Figures 6 and 10, when the temperatures of solutions are raised from 0 to 40 $^{\circ}$ C, the $\log(I_{650}/I_{456})$ value was reduced from 1.15 to ca. 0.65, and the fluorescence lifetime of RY3 at 650 nm was shortened from 711 to 183 ps. Essentially the same results were obtained in living NIH-3T3 cells, as demonstrated in SI Figures S13 and S14. The ratio values (SI Figure S13B) are clearly lower and fluorescence lifetimes of RY3 (SI Figure S14B) are similarly shortened. Therefore, the two modes of imaging give similar viscosity results in living cells.

Although the live cells are very complicated, with the spatial resolution of a confocal microscope via a simple calibration, we can correlate the two-mode results and let them work together to give reliable and accurate intracellular viscosity images previously unavailable.

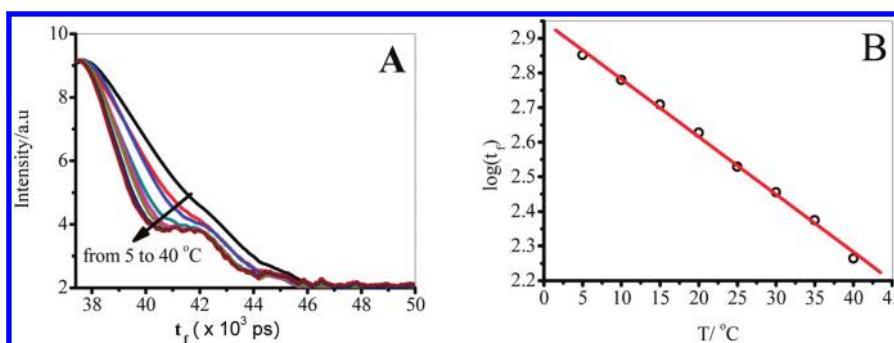


Figure 10. Fluorescence decays of RY3 (1.0 μ M) in 70/30 glycerol–ethanol solution with the increase of temperature at 650 nm (with a Horiba Jobin Yvon Fluoromax-4p system excited at 376 nm) (A); and Inverse linearity between $\log \tau_f$ and temperature (B).

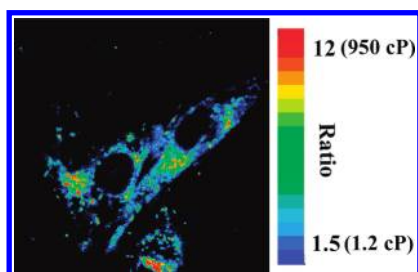


Figure 11. The fluorescence ratio image of MCF-7 cells stained by RY3 (5.0 μ M) observed under a Leica TCS-SP2 confocal fluorescence microscope (100 \times objective lens) at 18 $^{\circ}$ C and excited at 800 nm; the ratio image was obtained by image analysis software of Image Pro-plus 6.0.

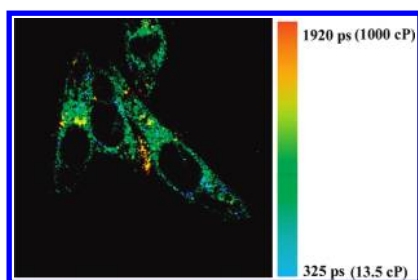


Figure 12. Fluorescence lifetime image of RY3 (5.0 μ M) in MCF-7 cells under TCSPC FLIM equipment: SPC150, excited at 800 nm, at 18 $^{\circ}$ C.

CONCLUSIONS

In conclusion, RY3, with a CHO group at the *meso*-position of the pentamethine chain, has low fluorescence quantum yields in nonviscous solutions. It is argued that the reason for this is that rotation of the CHO group releases the energy of the excited dye molecule nonradiatively via internal conversion including an ICT process. In viscous media, however, the rotation is restrained and large fluorescence enhancement was observed. A similar effect was obtained by lowering the temperature. The mechanism has been interpreted by ^1H NMR at low temperature and Theoretical calculation (Gaussian 09 software). Both the increase of viscosity and fall of temperature determine the rotation rates, resulting in ratio performance and lifetime increase. RY3 can enter into living cells and image intracellular viscosity by two modes of fluorescence ratiometry imaging and fluorescence lifetime imaging (FLIM). The accuracy and reliability of this application have been illustrated by comparison and correlation of the two images

in NIH-3T3 cells. To our best knowledge, RY3 is the first molecule providing the dual mode fluorescence responses, which will arouse more attention to discover more sensors to investigate cellular viscosity related to diseases and pathology.

ASSOCIATED CONTENT

S Supporting Information. Synthesis, experimental details, and additional spectroscopic data and images. This material is available free of charge via the Internet at <http://pubs.acs.org>.

AUTHOR INFORMATION

Corresponding Author

pengxj@dlut.edu.cn

ACKNOWLEDGMENT

This work was supported by NSF of China (20725621, 20876024, 21076032, 21072024, and 21006009), National Basic Research Program of China (2009CB724706), Ministry of Education of China, Cultivation Fund of the Key Scientific and Technical Innovation Project (707016).

REFERENCES

- (1) Stutts, M. J.; Canessa, C. M.; Olsen, J. C.; Hamrick, M.; Cohn, J. A.; Rossier, B. C.; Boucher, R. C. *Science* **1995**, 269, 847–850.
- (2) Luby-Phelps, K. *Int. Rev. Cytol.* **2000**, 192, 189–221.
- (3) Kaliviotis, E.; Yianneskis, M. *Proc. Inst. Mech. Eng., Part H* **2007**, 221, 887.
- (4) Phelps, K. L.; Mujumdar, S.; Mujumdar, R. B.; Ernst, L. A.; Galbraith, W.; Waggoner, A. S. *Biophys. J.* **1993**, 65, 236–242.
- (5) Haidekker, M. A.; Theodorakis, E. A. *Org. Biomol. Chem.* **2007**, 5, 1669–1678.
- (6) Haidekker, M. A.; Brady, T. P.; Lichlyter, D.; Theodorakis, E. A. *J. Am. Chem. Soc.* **2006**, 128, 398–399.
- (7) Fischer, D. E.; Theodorakis, A.; Haidekker, M. A. *Nature Protocols* **2007**, 227–236.
- (8) Kuimova, M. K.; Yahiolu, G.; Levitt, J. A.; Suhling, K. *J. Am. Chem. Soc.* **2008**, 130, 6672–6673.
- (9) Kuimova, M. K.; Botchway, S. W.; Parker, A. W.; Balaz, M.; Collins, H. A.; Anderson, H. L.; Suhling, K.; Ogilby, P. R. *Nature Chem.* **2009**, 1, 69–73.
- (10) Suhling, K.; French, P. M. W.; Phillips, D. *Photochem. Photobiol. Sci.* **2005**, 4, 13–22.
- (11) Zhang, J. F.; Zhou, Y.; Yoon, J.; Kim, Y.; Kim, S. J.; Kim, J. S. *Org. Lett.* **2010**, 12, 3852–3855.
- (12) Zhou, Y.; Wang, F.; Kim, Y.; Kim, S.; Yoon, J. *Org. Lett.* **2009**, 11, 4442–4445.

- (13) Levitt, J. A.; Kuimova, M. K.; Yahiolu, G.; Chung, P. H.; Suhling, K.; Phillip, D. *J. Phys. Chem. C* **2009**, *113*, 11634–11642.
- (14) Ock, K.; Jang, G.; Roh, Y.; Kim, S.; Kim, J.; Koh, K. *Microchem. J.* **2001**, *70*, 301–305.
- (15) Zoppellaro, G.; Geies, A.; Enkelmann, V.; Baumgarten, M. *Eur. J. Org. Chem.* **2004**, 2367–2374.
- (16) Shao, F. W.; Weissleder, R.; Hilderbrand, S. A. *Bioconj. Chem.* **2008**, *19*, 2487–2491.
- (17) Frisch, M. J. et al. Gaussian 09, Revision A.02, Gaussian, Inc., Wallingford CT, 2009.
- (18) Zhou, L. C.; Zhao, G. J.; Liu, J. F.; Han, K. L.; Wu, Y. K.; Peng, X. J.; Sun, M. T. *J. Photochem. Photobiol. A: Chemistry* **2007**, *187*, 305–310.
- (19) Dreizler, M. R.; Gross, E. K. U. *Density Functional Theory*; Springer Verlag: Heidelberg, 1990.
- (20) Gross, E. K. U.; Kohn, W. *Phys. Rev. Lett.* **1985**, *55*, 2850–2852.
- (21) Stratmann, R. E.; Scuseria, G. E.; Frisch, M. J. *J. Chem. Phys.* **1998**, *109*, 8218–8224.
- (22) Velapoldi, R. A.; Tönnesen, H. H. *J. Fluoresc.* **2004**, *14*, 465–472.
- (23) Reichardt, C.; Grah, W. *Tetrahedron* **1976**, *32*, 125–134.
- (24) Reichardt, C.; Mormann, W. *Chem. Ber.* **1972**, *105*, 1815–1839.
- (25) Haidekker, M. A.; Brady, T. P.; Lichlyter, D.; Theodorakis, E. A. *Bioorg. Chem.* **2005**, *33*, 415–425.
- (26) Förster, Th.; Hoffmann, G. Z. *Phys. Chem.* **1971**, *75*, 63–76.
- (27) Li, H. L.; Fan, J. L.; Wang, J. Y.; Tian, M. Z.; Du, J. J.; Sun, S. G.; Sun, P. P.; Peng, X. J. *Chem. Commun.* **2009**, 5904–5906.
- (28) Lee, K. S.; Kim, T. K.; Lee, J. H.; Kim, H. J.; Hong, J. I. *Chem. Commun.* **2008**, 6173.
- (29) Chen, X. Q.; Zhou, Y.; Peng, X. J.; Yoon, J. *Chem. Soc. Rev.* **2010**, *39* (6), 1861–2336.
- (30) Touchkine, A.; Kraynov, V.; Hahn, K. J. *Am. Chem. Soc.* **2003**, *125*, 4132–4145.
- (31) Renikuntla, B. R.; Rose, H. C.; Eldo, J.; Waggoner, A. S.; Armitage, B. A. *Org. Lett.* **2004**, *6*, 909–912.
- (32) Song, B.; Zhang, Q.; Ma, W. H.; Peng, X. J.; Fu, X. M.; Wang, B. S. *Dyes Pigm.* **2009**, *82*, 396–400.
- (33) Song, F. L.; Peng, X. J.; Lu, E. H.; Zhang, R.; Chen, X. Y.; Song, B. J. *Photochem. Photobiol. A* **2004**, *168*, 53–75.
- (34) Fabian, J. *Chem. Rev.* **1992**, *92*, 1197–1226.
- (35) Leevy, W. M.; Gammon, S. T.; Smith, B. D. *J. Am. Chem. Soc.* **2006**, *128*, 16476.
- (36) Zhu, M.; Yuan, M.; Liu, X.; Xu, J.; Lv, J.; Huang, C.; Liu, H.; Li, Y.; Wang, S.; Zhu, D. *Org. Lett.* **2008**, *10*, 1481–1484.
- (37) Tang, B.; Yu, F. B.; Li, P.; Tong, L. L.; Duan, X.; Xie, T.; Wang, X. J. *Am. Chem. Soc.* **2009**, *131*, 3016–3023.
- (38) Gruber, H. J.; Hahn, C. D.; Kada, G.; Riener, C. K.; Harms, G. S.; Ahler, W.; Dax, T. G.; Knaus, H. G. *Bioconj. Chem.* **2000**, *11*, 696–704.
- (39) Weissleder, R.; Ntziachristos, V. *Nat. Med.* **2003**, *9*, 123–131.
- (40) Peng, X. J.; Song, F. L.; Lu, E. H.; Wang, Y. N.; Zhou, W.; Fan, J. L.; Gao, Y. L. *J. Am. Chem. Soc.* **2005**, *127*, 4170–4171.
- (41) Kiyose, K.; Kojima, H.; Nagano, T. *J. Am. Chem. Soc.* **2006**, *128*, 6548–6549.
- (42) O'Connor, D. V.; Phillips, D. *Time-Correlated Single-Photon Counting*; Academic Press: London, 1984.
- (43) Becker, W. *Advanced Time-Correlated Single Photon Counting Techniques*; Springer: Berlin, 2005.